THE JOURNAL OF COMPARATIVE NEUROLOGY 493:460–474 (2005)

Gene Expression Differences over a Critical Period of Afferent-Dependent Neuron Survival in the Mouse Auditory Brainstem

JULIE A. HARRIS, NATALIE A. HARDIE, OLIVIA BERMINGHAM-McDONOGH, AND EDWIN W RUBEL*

Virginia Merrill Bloedel Hearing Research Center, Department of Otolaryngology, Head and Neck Surgery, and Graduate Program in Neurobiology and Behavior, University of Washington, Seattle, Washington 98195

ABSTRACT

Deprivation of auditory nerve input in young mice results in dramatic neuron death in the anteroventral cochlear nucleus (CN), while the same manipulation performed in older mice does not result in significant neuronal loss. The molecular basis underlying this critical period of susceptibility to loss of afferent input remains largely unknown. One possibility is that developmental differences in baseline mRNA expression of specific genes could predispose CN neurons to either death or survival after deafferentation. We used two microarray platforms to identify differentially expressed genes in the CN during and after this critical period. Results across platforms were also compared to each other. Three ages were examined; during the critical period (postnatal day (P)7), at the closing of the critical period (P14), and 1 week after the critical period (P21). Of all the genes surveyed (22,690 or 15,247), 1,082 were identified as significantly changed in expression during the critical period relative to after. Real-time reverse transcription polymerase chain reaction and immunohistochemistry confirmed and extended the microarray results for a subset of these genes. Further analysis of genes related to apoptotic pathways showed 6 out of 7 differentially expressed known pro-apoptotic genes had higher expression during the critical period. In contrast, 9 out of 11 differentially expressed known pro-survival genes increased after the critical period when CN neurons survive deprivation. This finding supports the concept that multiple neuroprotective mechanisms increase and pro-apoptotic factors decrease over development to protect mature neurons from stressful insults, making them less dependent on afferent input for survival. J. Comp. Neurol. 493:460–474, 2005.

Indexing terms: microarray; critical period; cochlear nucleus; deafferentation; apoptosis; gene expression

One poorly understood phenomenon in developmental neuroscience is how immature neurons highly sensitive to apoptotic stimuli mature into adult neurons that are more resistant to the same challenges. Neuron death induced by afferent deprivation is a dramatic example of an effect produced by removing sensory input during a critical period of development (Born and Rubel, 1985; Galli-Resta et al., 1993; Baldi et al., 2000). Later manipulations of afferent input have little or no effect on cell survival. The molecular bases of these critical periods of age-dependent susceptibility are essentially unknown in any system.

The auditory system has proven to be useful for studying the role of afferent input on neuron survival. Ablating the cochlea in young animals of several species results in rapid and profound changes in the brainstem cochlear nucleus (CN), including neuron death (Levi-Montalcini, 1949; Trune, 1982; Born and Rubel, 1985; Hashisaki and Rubel, 1989; Moore, 1990; Mostafapour et al., 2000). Cochlear ablation in older animals results in little or no neuron death in the CN. Interestingly, this change parallels the onset of hearing in all mammalian species studied.

Grant Sponsor: National Institute on Deafness and Other Communication Disorders; Grant number: DC03829; Grant number: DC04661; Grant number: DC07001; Grant sponsor: Garnett Passe and Rodney Williams Memorial Foundation.

Natalie A. Hardie's present address is Department of Otolaryngology, The University of Melbourne, Parkville, Victoria 3052, Australia.

This article includes Supplementary Material available via the Internet at http://www.interscience.wiley.com/jpages/0021-9967/suppmat.

*Correspondence to: Edwin W Rubel, Virginia Merrill Bloedel Hearing Research Center, Box 357923, CHDD Bldg, Rm CD176, University of Washington, Seattle, WA 98195-7923. E-mail: rubel@u.washington.edu

Received 19 April 2005; Revised 13 June 2005; Accepted 14 July 2005

DOI 10.1002/cne.20776

Published online in Wiley InterScience (www.interscience.wiley.com).

In the young postnatal mouse, anteroventral CN neurons undergo an apoptotic-like process following deprivation. Caspase 3 activation peaks within 12 hours and 30–60% cell death occurs by 96 hours (Mostafapour et al., 2000, 2002). Although there is a gradual decline in the maximal amount of neuron death as a result of cochlear ablation between postnatal day (P) 5 and P11, by P14 the same manipulation results in less than 1% neuron loss in the anteroventral CN. Therefore, this critical period ends after P11 and before P14 in the mouse. A more abrupt end to this critical period has been described in the gerbil CN (Tierney et al., 1997).

The molecules responsible for both age-dependent susceptibility and later protection of CN neurons remain largely unknown. It seems implicit that a developmental switch occurs in either gene expression or function that defines the critical period window. Previous studies suggested the abundance of a known regulator of cell survival, Bcl-2, could underlie this switch from afferent-dependent to -independent survival (Mostafapour et al., 2000, 2002). However, we decided it was necessary and important to undertake an unbiased approach by surveying the expression of thousands of genes in the mouse CN using microarray technology. Specifically, we sought to identify genes with changes in constitutive mRNA expression at ages within and after the critical period to address the hypothesis that expression levels of particular genes may predispose CN neurons after cochlear ablation to either death during the critical period or survival after the critical period.

We used two microarray platforms, the Affymetrix Mouse 430A GeneChip and the National Institute of Aging (NIA) Mouse 15K cDNA microarray, to compare gene expression in the mouse CN during the critical period at P7, at the closing of the critical period at P14, and 1 week after the critical period ends at P21. Results show many changes in gene expression over the first 3 postnatal weeks, but most changes occur by P14, in parallel with the end of the critical period and the onset of hearing. We identified candidate genes and found a strong correlation between postnatal age and the relative expression of genes that either promote or protect against cell death.

MATERIALS AND METHODS

Animals

Mice of the C57Bl/6J strain were used at postnatal days 7, 14, and 21. Pups were considered 0 days (P0) on the day of birth. The University of Washington Animal Care and Use Committee approved all procedures.

Tissue dissection

Mice were decapitated and the skull opened to expose the brain. The cochlea was pulled away from the brainstem and the 8th nerve was cut. After removal of the overlying cerebellum, the CN was visualized and dissected out with fine curved-tip scissors bilaterally. Tissue was immediately frozen in liquid N_2 and stored at −80°C until RNA extraction. Figure 1 shows an example of thionin-stained brainstem sections from P7 and P21 mice with the CN dissected out on one side only.

Microarray platforms

A cDNA microarray spotted with the NIA mouse 15K clone set was used to directly compare P7 and P21 CN gene expression on the same microarray slide (n = 5 replicates) (Tanaka et al., 2000). The cDNA array was fabricated at the Fred Hutchinson Cancer Research Center (FHCRC) DNA Array Facility. An oligonucleotide array from Affymetrix (Santa Clara, CA), the Mouse Expression Set 430A GeneChip, was used for comparison of P7 (n = 3), P14 (n = 2), and P21 (n = 3) CN gene expression.

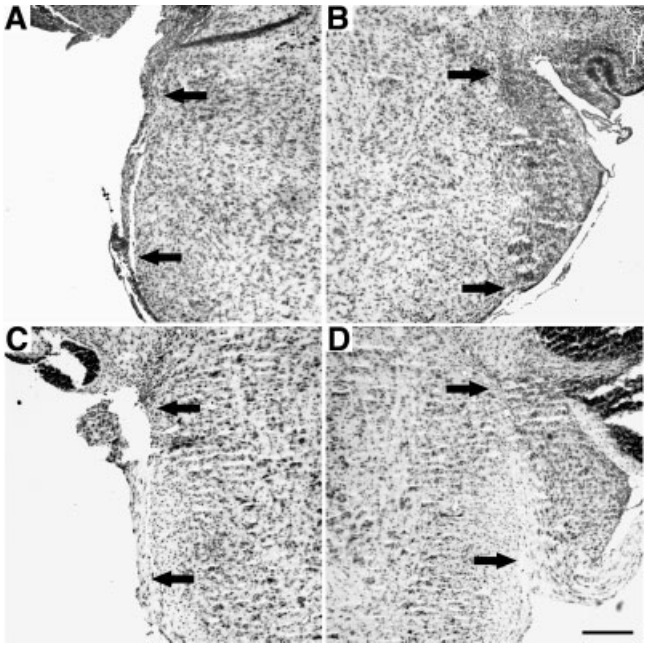

Fig. 1. Cochlear nucleus (CN) dissections. Representative thionin-stained sections through the level of the anteroventral cochlear nucleus (AVCN) after removal of the entire CN on one side of the brain. The CN was cleanly dissected away with little or no contamination from other brain structures shown in the left panels compared to the intact contralateral side shown in the right panels at P7 (**A,B**) and P21 (**C,D**). Arrows indicate the medial border of AVCN. Scale bar = 250 μm in D (applies to A–D).

Preparation of total RNA

Total RNA was isolated from samples of pooled cochlear nuclei and DNAse treated using the Qiagen (Valencia, CA) RNeasy Mini Kit with the on-column DNAse set. RNA concentration and integrity was assessed using an Agilent 2100 Bioanalyzer (Palo Alto, CA). Approximately 0.75 μg of total RNA was obtained per CN at any of the ages. Separate pools of CN tissue were isolated for each replicate sample. Forty cochlear nuclei were pooled to generate a minimum of 20 μg total RNA for the cDNA arrays. Ten cochlear nuclei were pooled to generate a minimum of 5 μg of total RNA for the Affymetrix arrays.

Linear amplification of RNA samples for cDNA arrays

Two out of five replicate analyses using the NIA Mouse 15K cDNA microarray were done with amplified RNA as the cDNA template instead of total RNA. Linear amplification of 5 μg of total RNA was performed using the RiboAmp RNA Amplification kit from Arcturus (Mountain View, CA). RNA concentration and integrity of the resulting antisense RNA (aRNA) was checked using the Agilent

2100 Bioanalyzer. We consistently obtained 30 μg of aRNA after one round of amplification. Comparison of microarray data derived from arrays hybridized using amplified RNA with total RNA showed a good correlation (r = 0.81) that improved when only genes of moderate to high abundance were considered (data not shown).

Preparation of labeled cDNA, hybridization, array scanning, and image analysis for the NIA mouse 15K cDNA microarray

The FHCRC DNA Array Facility performed the following procedures. The protocol used for cDNA labeling was a modification of a protocol described elsewhere (cmgm.stanford.edu/pbrown/protocols/aadUTPCouplingProcedure.htm). Briefly, labeled cDNA targets were prepared by reverse transcription of 20 μg of total RNA, or 5 μg of aRNA, using oligo(dT)18 primer in the presence of 0.2 mM 5-(3-aminoallyl)-2-deoxyuridine 5-triphosphate (Sigma-Aldrich, St. Louis, MO), 0.3 mM dTTP, and 0.5 mM each dATP, dCTP, and dGTP. Following cDNA synthesis, either Cy3 or Cy5 monoreactive fluor (Amersham Life Sciences, Arlington Heights, IL) was covalently coupled to the cDNA-incorporated aminoallyl linker in the presence of 50 mM sodium bicarbonate (pH 9.0). Two color expression profiles were generated using microarrays in which P7 and P21 cDNA targets were labeled with different fluors. In one of the replicates the dyes were reversed (dye flip control) to account for differences in hybridization due to the physical characteristics of each dye. Following cohybridization to the chip, a fluorescent image of the microarray was collected at both emission wavelengths using a GenePix 4000 fluorescence scanner (Axon Instruments, Foster City, CA), and image analysis was performed using GenePix3.0 microarray acquisition and analysis software. The quality of hybridizations and overall array performance was determined by visual inspection of the raw scanned image for artifacts or scratches. The median background-subtracted intensity at both Cy3 and Cy5 wavelengths for each spot on the microarray was uploaded into the software program Genesifter.net for further analyses (VizX Labs, Seattle, WA).

Preparation of labeled cRNA, hybridization, array scanning, and image analysis for the Affymetrix mouse expression set 430A GeneChip

The Center for Expression Arrays at the University of Washington performed the following procedures. Biotinylated labeled target cRNA was prepared and hybridized to the Mouse 430A GeneChip with minor modifications from the Affymetrix recommended procedures (affymetrix.com/support/technical/manual/expression_manual.affx).
Briefly, 5 μg total RNA was reverse-transcribed into double-stranded cDNA using a T7-(dT)24 primer in the presence of 10 mM dNTP mix and poly-A spike in positive control RNAs during first strand synthesis (Invitrogen, Carlsbad, CA). Double-stranded cDNA was then used as a template for synthesis of biotin-labeled cRNA (Enzo Diagnostics, Farmingdale, NY). Labeled cRNA was cleaned up to remove unincorporated NTPs and the concentration was determined spectrophotometrically. According to Affymetrix protocols, 15 μg of cRNA was then fragmented and transcript sizes were analyzed on the Bioanalyzer to be between 50 and 200 bp. Spike-in eukaryotic hybridization controls were added to the cRNA samples and hybridization to the GeneChips was performed for 16 hours at 45°C. Using the Affymetrix GeneChip System, arrays were then washed and stained with streptavidin-phycoerythrin (Molecular Probes Eugene, OR) and scanned using a GeneChip Scanner. The quality of hybridizations and overall chip performance was determined by visual inspection of the raw scanned data for artifacts, scratches, or bubbles. The Affymetrix GeneChip Operating System (GCOS) report file (*.RPT) was used to determine if the following statistics were within acceptable limits: 3′/5′ GAPDH and beta-actin ratios did not exceed 1.5, chip background and noise were below cut-off limits, and hybridization spike-in controls were present and in increasing intensities. Background and noise were similar across all arrays used for comparisons. Detailed descriptions of quality control metrics can be found in the Affymetrix Expression Technical Manual at affymetrix.com/support/technical/manual/expression_manual.affx. Using the raw image file in GCOS (.DAT), cell intensities were calculated and the resulting files (.CEL) containing intensity information for all probes on the arrays were uploaded into the software program Genesifter.net for further analyses.

Array data analysis

Normalization of the raw microarray data and determination of differential expression was done using Genesifter.net software. The cDNA array data were normalized by the global median intensity on each array. Robust multiarray average (RMA) normalization was performed on the Affymetrix GeneChips. In brief, RMA performs three operations specific to Affymetrix chips: global background normalization, across array normalization, and log2 transformation of "perfect match" oligonucleotide values (Irizarry et al., 2003).

We looked for differences in gene expression between P7 and P21 CN using the NIA mouse 15K cDNA array. Using Affymetrix Mouse 430A GeneChips we looked for differences between P7 and P21 CN, but also P7 and P14 as well as P14 and P21 CN. Lists of genes with different expression patterns were generated using two criteria: an adjusted *P*-value cut-off of ≤ 0.05 and a fold change threshold of ≥ 1.8. More specifically, a Student's *t*-test was performed on the replicate array intensity values (n = 5 cDNA arrays and n = 2, P14, or 3, P7 and P21, Affymetrix arrays). Because the probability of false identifications increases with the large number of genes tested, *P*-values were adjusted using the Benjamini and Hochberg procedure for controlling the false discovery rate (FDR) (Reiner et al., 2003).

In order to further explore changes in gene expression during (P7) and after (P14, P21) the critical period in the CN, an ANOVA was performed on all three groups on the Affymetrix arrays. The same criteria as above were used to determine genes changing in expression from P7 to P14 and P21. These genes (n = 1,512) were clustered using hierarchical methods to visualize changes in the CN over these ages, but also clustered using partitioning around medoids (PAM). Both of these methods showed that there were two major clusters in these data: genes that increased during the critical period at P7 over their expression at P14 or P21, and genes that increased after the critical period at P14 or P21 over their expression at P7. Because this was still a large number of genes the filtering

TABLE 1. Primer Sequences for Real-Time RT PCR

Gene name	Forward primer	Reverse primer	*Accession number*
14-3-3eta	ggagcgctacgacgatatg	cttgtaggccacagagaggag	*NM_011738*
αB Crystallin	tctctccggaggaactcaaa	tccggtacttcctgtggaac	*NM_009964*
Bcl-w	aagaaatggagcctttggtg	cccgtatagagctgtgaactcc	*NM_007537*
Bcl-x	cgtggaaagcgtagacaagg	gctgcattgttcccgtagag	*NM_009743*
BID	catctttgctccgtgatgtc	tgtcaccatcgggcttgt	*NM_007544*
Bok	gacgcttggcagaggtgt	gtcaccacaggctccgact	*NM_016778*
C-myc	ctctccttcctcggactcg	caccacatcaatttcttcctca	*NM_010849*
Calretinin	gagaaggcaaggaagggttc	tcttcggtcggcaggatc	*NM_007586*
Caspase 3	tcggtcttacagaccagcaa	ccaggaggaccgtcagatta	*U63720*
Caspase 7	cccaaactcttcttcattcagg	gcttccaccgggatcttgt	*NM_007611*
CDK5 (p35)	gctcaagcccttcctggt	aaatagtgtgggtcggcatt	*NM_009871*
Gelsolin	tgcaggaagacctggctact	ttgctggatctgtctcgatg	*NM_146120*
Glutamine synth.	ccagggaactggaatggtg	ggtactggtgcctcttgctc	*NM_008131*
Hsp105	aatgaggtgatggagtggatg	tgggttgagttacaacaggttc	*NM_013559*
Hrsp12	gtcgctgctttaccaagagg	gagtcaacatcagcatggctac	*NM_008287*
Metallothionein I	ctgtgcctgatgtgacgaac	tttattattcacgtactcggtagaaa	*BC036990*
p75	ggccttgtggcttatattgc	tgtcgctgtgcagtttctct	*NM_033217*
Parvalbumin	aagggcttctcctcagatgc	gtcagcgccacttagctttc	*NM_013645*
PI3K p85	caaagcggagaacctattgc	cggtggcagtcttgttaatg	*NM_011085*
PKA RII β	tattgttgagcccactgcat	catagccgaggcattcattt	*NM_011158*
Prion Protein	atcaccatcaagcagcacac	cttctcccgtcgtaataggc	*NM_011170*
RPL3	tcattgacaccacctccaaa	gcacaaagtggtcctggaat	*NM_013762*
Waf (P21)	gtctgagcggcctgaaga	tctgcgcttggagtgataga	*NM_007669*

criteria were made stricter. Critical period candidate genes had to be significantly increased in the P7 CN over both P14 and P21. Conversely, postcritical period candidate genes had to be significantly increased in both the P14 and P21 CN over P7. The entire dataset from both microarray platforms has been deposited in the Gene Expression Omnibus under the series number GSE2390 (www.ncbi.nlm.nih.gov/geo/).

Real-time reverse transcription polymerase chain reaction

Real-time reverse transcription polymerase chain reaction (RT-PCR) was performed on a BioRad (Hercules, CA) iCycler System using SYBR Green detection. cDNA template was made from 1 μg total RNA extracted from P7 or P21 CN using the BioRad iScript cDNA Synthesis kit. The 25 μl PCR reactions contained 12.5 μl SYBR green Supermix, 5 μl cDNA template, 0.375 μl each of the forward and reverse primers (800 nM), and 6.75 μl water. The conditions were 95°C for 3 minutes followed by 45 cycles of denaturing at 95°C for 30 seconds, and annealing and extension at 54°C for 30 seconds. Melt curves were also analyzed to insure only one product per well. Primer sequences were designed using the Primer3 software available online (frodo.wi.mit.edu) and ordered from Integrated DNA Technologies (Coralville, IA). Primer sequences and GenBank accession numbers for the genes selected for PCR validation are shown in Table 1. The gene chosen as a control for these experiments was the ribosomal protein L3 (RPL3). This gene was chosen over more standard genes such as GAPDH or beta-actin because those genes appeared to increase slightly over development in the CN based on the microarray data. RPL3 showed no change between P7 and P21 and is relatively highly expressed in the CN. An initial dilution series was performed with each template cDNA for all primer sets to determine their PCR efficiency. Each reaction was then done in triplicate wells on one plate, and then the plate was duplicated or triplicated. We used the comparative C_T method of relative quantification, where C_T = threshold cycle, the cycle at which fluorescence is just measurable above baseline (baseline was user-defined to minimize standard deviation of replicate wells; this was always higher than the software default value and kept constant across all plates for C_T measurements). In this method the equation $\Delta\Delta C_T = \Delta C_T(P7) - \Delta C_T(P21)$ was used to determine the amount of target in one sample versus the other, where ΔC_T is $C_T(\text{gene}) - C_T(\text{RPL3})$. $2^{-\Delta\Delta Ct}$ then gives the relative amount of target gene.

Histology and immunohistochemistry

Mice were overdosed with sodium pentobarbital and perfused transcardially with 4% paraformaldehyde. After perfusion the brains were removed and postfixed for an additional 2 hours at room temperature (RT), then serially dehydrated in ethanol, cleared in methyl salicylate, and embedded in paraffin. A one-in-five series of 10-μm coronal sections was mounted on slides. To assess completeness of the CN dissections, brain sections were deparaffinized in xylenes, rehydrated in alcohols, and stained with thionin. For immunohistochemistry, sections were deparaffinized and rinsed in 0.01% Triton-X in phosphate-buffered saline (PBST) for 15 minutes. Antigen retrieval was performed in 10 mM citric acid (pH 6.0) in a steamer for 25 min, and then cooled for 10 minutes on ice. Slides were rinsed again in PBST for 15 minutes and then blocked for 1 hour at RT in 10% normal serum, 0.1% Triton-X, and 0.5% bovine serum albumin in PBS. Sections were next incubated overnight at 4°C with the primary monoclonal antibody: mouse anti-αB crystallin (1:500, StressGen Biotechnologies, #SPA-222, San Diego, CA), mouse anti-metallothionein I/II (1:1000, StressGen Biotechnologies, #SPA-550), mouse anti-parvalbumin (1:1,000, Sigma-Aldrich, #P 3088), mouse anti-PKA II regulatory subunit β (1:100, BD Biosciences, #610625, San Jose, CA), mouse anti-procaspase 3 (1:80, BD Biosciences, #611048), or mouse anti-cmyc (1:100, Santa Cruz Biotechnology, #sc-40, Santa Cruz, CA). The next day tissue was rinsed for 30 minutes in PBST and incubated in biotinylated goat antimouse secondary antibody (1:200, Vector Laboratories, Burlingame, CA) for 1 hour at RT. After rinsing for another 15 minutes in PBST, tissue was incubated in Vector avidin-biotin complex solution for 1 hour at RT. The tissue was rinsed again for 15 minutes in PBS and reacted with diaminobenzidine (Sigma). Slides were

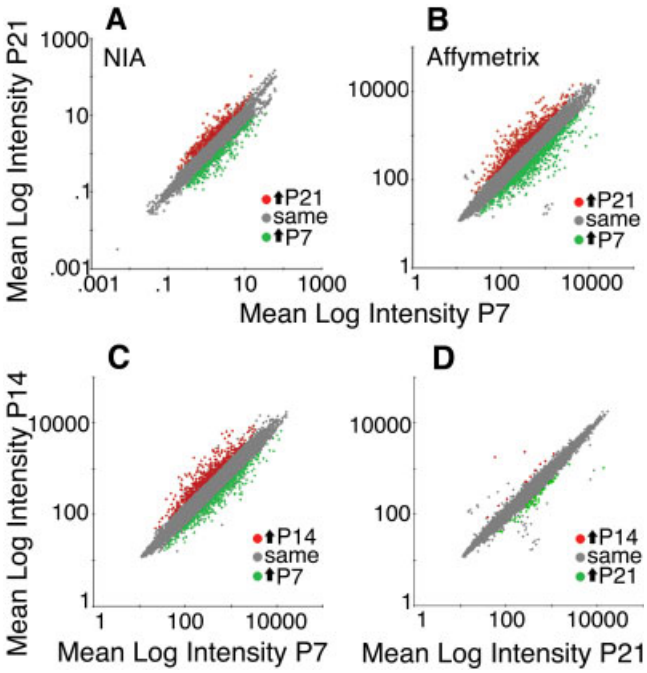

Fig. 2. Scatterplots showing differentially expressed genes in the CN from both the Affymetrix and NIA microarrays. Differential expression was defined as ≥ 1.8 fold change ratio and a false discovery rate adjusted *P*-value ≤ 0.05 after a *t*-test. The mean log intensity at P21 for probes represented on the arrays was plotted against P7 from the NIA (**A**) or Affymetrix microarray (**B**). Mean log intensities for P14 CN (Affymetrix only) are plotted against P7 (**C**) and P21 (**D**). Differentially expressed genes are shown in green or red and genes that were unchanged between the age comparisons are shown in gray. Note that by these criteria many genes are differentially expressed between P7 and P14 or between P7 and P21, but very few genes are differentially expressed between P14 and P21. N = 5 replicates (NIA, A), 2 replicates (Affymetrix P14, C,D), and 3 replicates (Affymetrix, P7 and P21, B–D).

then washed, dehydrated, and coverslipped with DPX (BDH Laboratories, Poole, UK).

Positive controls were run for two antibodies (gut tissue: caspase 3, lens: αB crystallin) and negative (primary omission) controls were included with all immunohistochemistry. The immunogens used to generate these antibodies were as follows: αB crystallin, purified from bovine eye lens; metallothionein I/II, cross-linked rabbit liver MT-I and MT-II; parvalbumin, purified from frog muscle; PKA II regulatory subunit β, from human amino acids 1–418 of PKA II regulatory subunit β gene; pro-caspase 3, amino acids 25–145 of mouse caspase 3 gene; and c-myc, amino acids 408–439 within the C-terminal domain of the human c-myc gene. The antibody manufacturers' have confirmed the specificity of each antibody using Western blot analyses in several species, including rat and mouse. The antibodies recognize the following protein masses that are the appropriate molecular weight: αB crystallin, 20 kDa protein; metallothionein I/II, 15 kDa protein (although additional higher weight proteins are also detected that may correspond to aggregates of metallothionein); parvalbumin, 12 kDa protein; PKA II regulatory subunit β, 53 kDa protein; pro-caspase 3, 32 kDa protein as well as the p17 cleaved form of active caspase 3; and c-myc, 67 kDa protein.

TABLE 2. Numbers of Differentially Expressed Genes on Both Array Platforms

	Increased during the critical period at P7	Increased after the critical period at P14 or P21
Affymetrix		
P21 vs. P7	823	589
P14 vs. P7	415	461
P21 and P14 vs. P7	380	273
NIA		
P21 vs. P7	257	273
NIA and Affymetrix		
Shared genes	102	107
Genes unique to Affymetrix	278	274
Genes unique to NIA	155	166
Total candidates	535	547

Listed are the numbers of genes showing at least a 1.8-fold increase and an FDR adjusted *P*-value ≤ 0.05 between P7, P14, and P21 for both the Affymetrix and NIA cDNA microarray comparisons. For the Affymetrix arrays, critical period candidate genes had to be increased at P7 compared to both P14 and P21, and postcritical period genes had to be increased at P14 and P21 compared to P7. The Affymetrix genes and NIA genes were combined to make a final list containing unique candidates.

Photomicrographs were taken using a CoolSnap HQ Digital Camera (Photometrics, Tucson, AZ) under a 4×, 20×, or 63× objective on a Zeiss Axioplan 2 microscope. Images were captured using Slidebook 4.0 software (Intelligent Imaging Innovations, Santa Monica, CA). All photomicrograph figures were prepared using PhotoShop 7.0 (Adobe Systems, San Jose, CA) and for some images the dodging tool was used to correct uneven illumination.

RESULTS

Identification of differentially expressed genes on the microarrays

Changes in relative gene expression in the mouse CN during and after a critical period of afferent-dependent survival were broadly evaluated using both cDNA and oligonucleotide microarrays. In the NIA 15K mouse cDNA microarray analysis, gene expression in the P7 CN was compared with the P21 CN. Using Affymetrix GeneChips, P7, P14, and P21 CN gene expression were compared. Differentially expressed genes were identified by having at least a 1.8-fold change and a false discovery rate (FDR) adjusted *P*-value ≤ 0.05 after a *t*-test. Scatterplot analyses of all the microarray comparisons are shown in Figure 2. The numbers of differentially expressed genes for the comparisons in Figure 2A–C are also shown in Table 2. Of the 15,247 genes represented on the NIA 15K microarray, 273 genes (0.018%) were expressed more highly after the critical period at P21 compared to P7 and 257 genes (0.017%) were expressed more highly during the critical period at P7 compared to P21 (Fig. 2A). Of the 22,690 genes represented on the Affymetrix arrays, 589 genes (0.026%) showed increased expression and 823 genes (0.036%) decreased at P21 relative to P7 (Fig. 2B); 461 genes (0.020%) showed increased expression and 415 genes (0.018%) decreased at P14 relative to P7 (Fig. 2C). Interestingly, only 21 genes (0.001%) showed increased expression and 9 genes (0.0004%) decreased when we compared P21 relative to P14 CN (Fig. 2D).

The Affymetrix data including P7, P14, and P21 were analyzed by hierarchical clustering to identify possible

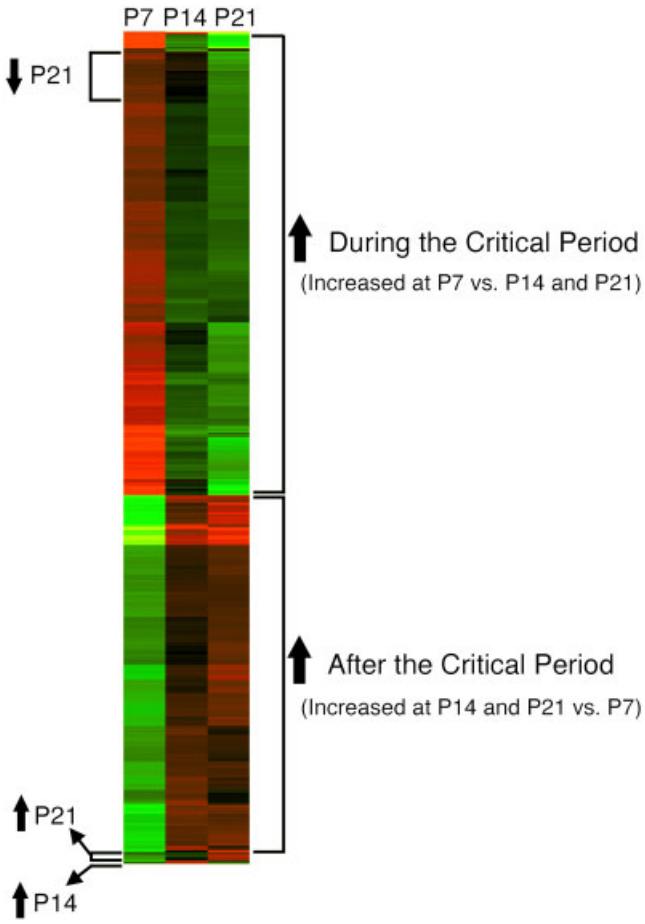

Fig. 3. Hierarchical cluster analysis of genes differentially expressed at P14 or P21 relative to P7. All nonregulated genes were eliminated from this analysis. Each column represents one age, each row a single gene. Red, expression of that gene is higher than the mean intensity of all three ages; black, equal to the mean; green, expression is lower than the mean. A cluster is a group of genes with a similar pattern of expression (i.e., colors in this figure) across the three ages. Two major clusters were identified, 1) increased during the critical period (P7) or 2) increased after the critical period (P14 and P21). Very few genes followed other expression patterns over these ages. Much smaller clusters included genes that showed decreased expression at P21 compared with both P7 and P14, increased expression at P21 over both P7 and P14, and a small subset of genes that showed higher expression at P14 over both P7 and P21.

correlations in expression patterns in the CN, shown in Figure 3. Only genes that were differentially expressed in either P14 or P21 compared with P7 CN were used for this analysis. Remarkably, only two major clusters appeared, genes that were increased during the critical period (P7 > P14 and P21) and genes that were increased after the critical period (P14 and P21 > P7). There were very few genes that did not fit into these two groups, although some smaller clusters can be identified. In accordance with Figure 2D, this analysis suggests that the vast majority of changes in CN gene expression over postnatal development occur during the second postnatal week, a period that encompasses the end of the critical period and the onset of hearing. We find this of considerable interest in view of the fact that dramatic changes in neuronal responses to acoustic stimulation are still occurring over the third postnatal week, especially since many of these changes take place at the level of the cochlea, thereby radically changing the amount and patterns of activity impinging on the CN (Sanes and Walsh, 1998).

Comparison of fold change measured for genes shared on both platforms

Results from several published technical articles show an overall low correlation between fold change ratios measured for the same genes on different microarray platforms (Kuo et al., 2002; Park et al., 2004). Therefore, we felt it was important to determine the amount of correlation in our datasets. Using Genesifter software all probes with the same UniGene ID on both arrays were identified and matched. We found 5,159 unique UniGene entries, consisting of 7,592 cDNA probes and 9,452 Affymetrix probes. When multiple probes matched the same UniGene ID, their values were averaged (although the extent of agreement between probes supposedly measuring the same gene is not always good, the unaveraged data showed only a slightly improved correlation). We compared the fold change of P7 compared to P21 for all these shared genes on both array platforms (Fig. 4A). There was a weak, but positive, correlation ($r = 0.613$). Because the overall correlation would be highly influenced by noisy data from low-intensity genes, we also computed the correlation coefficient separately for low- to high-intensity genes (Fig. 4B). The average intensity of each gene across all replicates and both platforms was put into 10 bins of equal size. The correlation coefficient increased as the signal intensity increased, from 0.263 in the lowest intensity bin to 0.951 at the highest intensity bin. The correlation coefficient was also calculated separately for genes showing no change between P7 and P21 samples (low fold change ratio) to the highest fold change (Fig. 4C). All shared genes were placed into four bins of equal size, ranging from the lowest average fold change to the highest average fold change across all replicates and both platforms. Absolute values were used so the direction of the change was not taken into account. The correlation improved with increasing fold change. Importantly, the highest correlations were obtained for genes that showed a fold change of greater than 1.8 ($r > 0.824$), which was part of our selection cutoff to determine robust differences in gene expression during and after the critical period. Figure 4B,C clearly shows that fold change estimates of moderate to highly expressed genes, and genes showing larger fold change ratios can be strongly correlated across platforms, even better than the overall correlation coefficient might suggest.

Identification and functional distribution of critical period candidate genes

The lists of differentially expressed genes from the Affymetrix dataset and the NIA 15K dataset were combined to form a cohesive list of possible critical period candidate genes. This resulted in a set of 535 unique genes more highly expressed during than after the critical period (P7 > P14 and P21), and 547 unique genes more highly expressed after the critical period relative to during the critical period (P14 and P21 > P7). Table 2 provides the details of this analysis.

Analyzing changes in broad functional groups provided some biological insight into these lists. The differentially

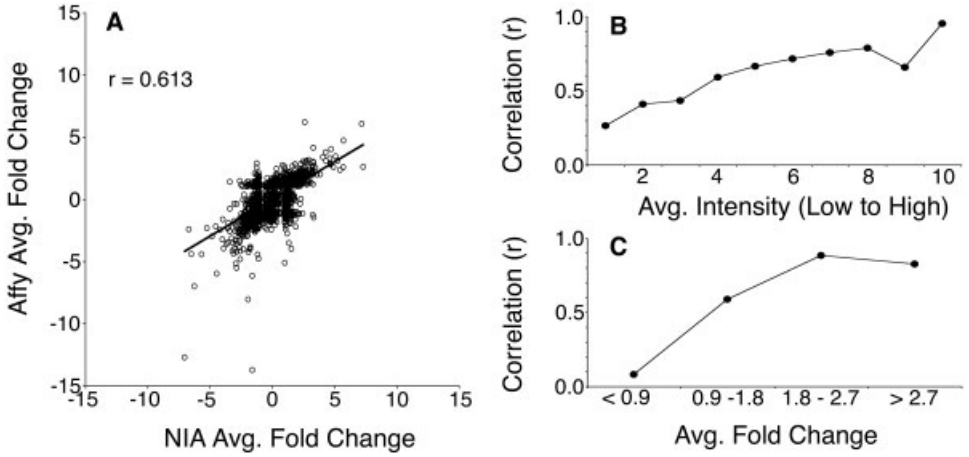

Fig. 4. Analysis of the correlation between fold change ratios for P7 compared to P21 CN for genes represented in both the Affymetrix and NIA datasets. **A:** Average fold change is plotted for all 5,169 genes shared on both platforms. **B:** The correlation coefficient between fold changes on Affymetrix and NIA arrays was computed and plotted on the y-axis for each of 10 bins containing genes with the lowest (Bin 1) to highest (Bin 10) expression level averaged across all replicates and both platforms shown on the x-axis. **C:** The correlation coefficient between fold changes on Affymetrix and NIA arrays was computed and plotted on the y-axis for each of four bins containing genes with the lowest average fold change ratios across replicates and platforms (<0.9) up to the highest average fold change ratios (>2.7). Note that increases in both expression level and fold change ratio remarkably improved the correlation coefficient.

expressed genes were classified into 15 different functional groups, shown in Figure 5, based on information from Kargul et al. (2001), the available literature, and the GeneOntology Consortium (Ashburner et al., 2000). The unknown group contains both expressed sequence tags as well as known genes with no clear function described in the literature. Figure 5A,B shows the functional groups that were most highly represented during and after the critical period on the Affymetrix and NIA microarrays. For example, the highest percentage of genes showing increased expression during the critical period at P7 were involved in unknown functions (29.3%), followed by roles in signal transduction (16.9%), transcription (12.7%), and matrix or structural genes (10.1%). The highest percentage of genes showing increased expression after the critical period at P14 and P21 also included those with unknown functions (24.1%) and signal transduction roles (23.7%), but unlike the increases at P7, energy and metabolism genes were also highly represented (14.6%). Importantly, these same trends in similarities and differences were observed in both the Affymetrix and NIA datasets (compare Fig. 5A,B). In Figure 5A,B a trend is also apparent in that the functional groups with the largest number of genes during the critical period are also the largest after the critical period (e.g., signal transduction), and the functional groups with the smallest number of genes are for the most part the same groups during and after the critical period (e.g., apoptosis and immune).

Relative changes in the predominance of functional groups during and after the critical period were also analyzed. In Figure 5C the difference between the percent of total genes increased during the critical period subtracted from after the critical period is plotted for each functional category and for each platform. The functional groups showing a higher percentage of total genes increased after the critical period at P14 or P21 compared to the group of critical period genes are shown as positive values. The functional groups with a higher percentage of genes increased during the critical period at P7 relative to after the critical period are shown as negative values. Functions overrepresented in the critical period group compared to the postcritical period group include apoptosis, cell cycle, DNA replication and repair, matrix or structural, protein synthesis, noncoding RNAs, or transcription. Functions overrepresented in the postcritical period are energy and metabolism, heat shock, immune, ion transport, proteolysis, signal transduction, and transport. Importantly, for all of the functional groups, with the exception of the unknowns, the direction of change was the same across the platforms. Together with our finding of a strong correlation between the fold changes measured for differentially expressed genes on both platforms (Fig. 4C), this analysis suggests that gene expression data can be confidently compared across these platforms, at least for genes with robust differences in expression ratios.

We sought to identify candidate genes on these lists that could specifically underlie the age-dependent response of death or survival following deafferentation of CN neurons. Accordingly, one way to further refine these lists of genes was to select genes with a previously known role in cell death or survival based on the published literature. In this way, 27 genes expressed higher during the critical period and 39 genes expressed higher after the critical period were selected as candidates for further study. We purposefully selected genes with pro-death functions during the critical period and pro-survival functions after the critical period in order to narrow down the lists and generate new hypotheses. However, it is of interest to note that we identified four genes with pro-death functions expressed higher after the critical period and five genes with pro-survival functions during the critical period (data not shown). Although this selection criterion is biased toward molecules that are known to play a role in cell death, not all of the genes were classified in the apoptotic functional group.

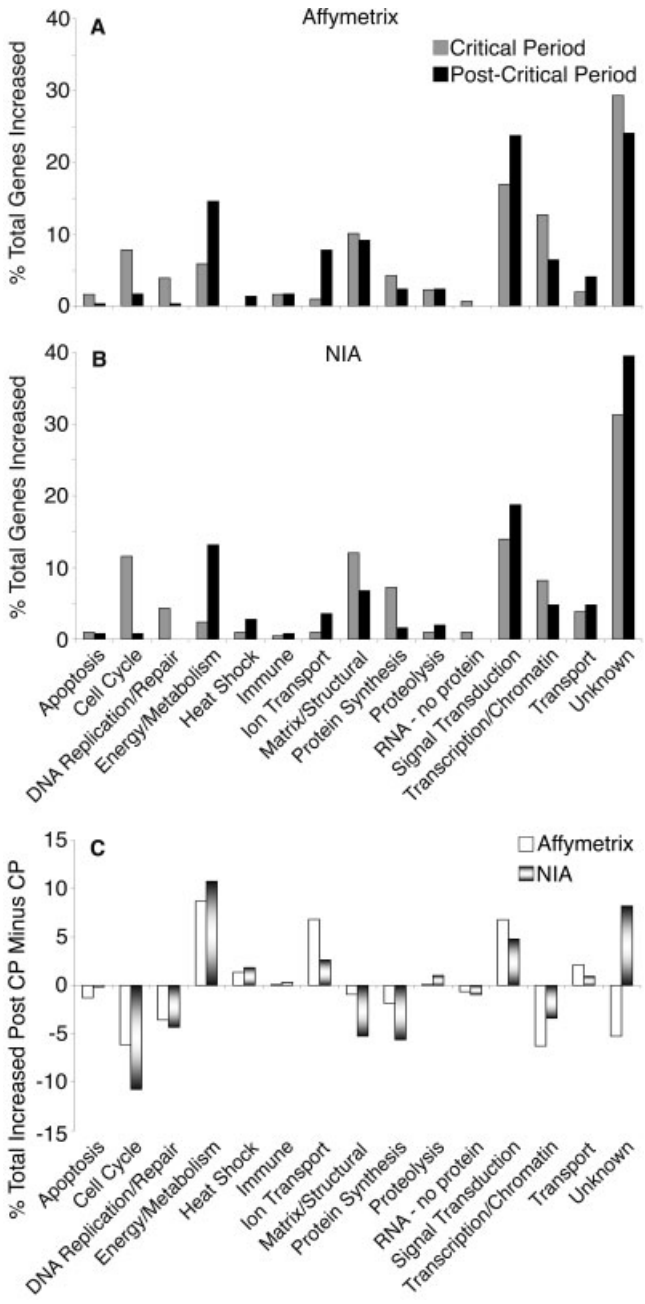

Fig. 5. Distribution of functional categories of differentially regulated genes during (P7) and after (P14 and P21) the critical period. Differentially expressed genes that were increased during the critical period (gray) or postcritical period (black) were categorized into 15 functions for the Affymetrix (**A**) and NIA (**B**) datasets. The percentage of total genes increased in each category is plotted on the y-axis. The functional categories showing the largest increases were similar across platforms. **C:** The difference between the percentage of total genes increased after the critical period and during the critical period for each functional category is plotted for both the Affymetrix and NIA datasets. The functional categories represented greater during the critical period (negative values) included cell cycle, DNA replication and repair, matrix and/or structural proteins, protein synthesis, and transcription. The functional categories represented greater after the critical period (positive values) included energy and metabolism, heat shock, ion transport, and signal transduction. With the exception of the unknown group, all other functions changed in the same direction on both platforms.

Candidates that were expressed higher during the critical period at P7 than P14 and/or P21, shown in Table 3, included pro-apoptotic genes such as caspase 3, the Bcl-2 family member Bid (BH3 interacting death domain agonist), and the p75 nerve growth factor receptor, although p75 can also act in a protective way under certain circumstances (Bamji et al., 1998; Kalb, 2005). Based on studies that have suggested a link between neuronal apoptosis and the reactivation of cell cycle proteins, we also selected a number of cell cycle-related genes expressed more highly during the critical period. For example, inhibition of the cell cycle transcription factor Myb (myeloblastosis oncogene) can reduce serum deprivation-induced neuronal death (Liu et al., 2004). An extracellular matrix protein expressed higher during the critical period, milk fat globule-EGF factor 8 protein, recognizes phosphatidyl serine on the membrane of apoptotic cells and functions to bring them to phagocytes (Hanayama et al., 2002).

Genes that function as proteinases, calpain 7 and matrix metalloproteinase 9, showed increased expression during the critical period and inhibition of both of these proteins can protect against different forms of neurotoxicity (Jourquin et al., 2003; Gafni et al., 2004). Members of signal transduction pathways were also increased, such as the p35 activator of cyclin-dependent kinase 5 (CDK5). Inhibiting CDK5 can protect against apoptotic and necrotic neuron death (Weishaupt et al., 2003). Furthermore, both an endogenous inhibitor of protein kinase A (PKA), protein kinase inhibitor alpha, and a regulatory subunit of PKA, PKARIIβ, that can suppress its catalytic activity were increased during the critical period. As PKA is often a strong survival-promoting pathway in neurons, inhibiting PKA signal transduction may sensitize these neurons to death. Finally, a group of transcriptional regulators that can enhance cell death was increased during the critical period, including c-myc and the ligand-activated aryl-hydrocarbon receptor (Ahr). Ahr can regulate the expression of various genes, including the pro-apoptotic gene Bax and the presence of the Ahr gene predisposes hepatocytes to Fas-mediated apoptosis (Matikainen et al., 2001; Park et al., 2005).

On the list of 547 genes increased after the critical period, we focused on a subset of 39 genes determined to have some role in promoting cell survival (shown in Table 4). These included multiple genes that favor a more reduced state in cells and can act to protect against oxidative stress, such as glutathione synthetase, peroxiredoxin 6, selenoprotein X1, and oxidation resistance 1. Multiple creatine-related genes were found to be increased after the critical period; creatine kinase and two creatine synthesis enzymes, glycine amidinotransferase and guanidinoacetate methyltransferase. Creatine provides strong protection against neural excitotoxic and ischemic damage (Brustovetsky et al., 2001; Zhu et al., 2004). There was also a strong group of genes responsive to heat shock or stress, including heat shock protein (hsp) 105 and a member of the small hsp family, αB crystallin, both of which have been shown to inhibit apoptosis (Hatayama et al., 2001; Kamradt et al., 2001, 2002). Transcription of metallothionein (MT) I and II is also responsive to stress, and enhancing the expression of MTI and II can protect neurons from ischemia and apoptosis (Giralt et al., 2002; Natale et al., 2004).

Genes with a role in the transport of ions were also increased after the critical period at P14 and P21. The

TABLE 3. Candidate Genes Expressed Higher during the Critical Period[1]

Gene name	*Accession number*	NIA ratio P7/P21	Affy ratio P7/P14	Affy ratio P7/P21
Apoptosis				
BH3 interacting death domain agonist (BID)	*BC002031*	5.65	1.84	2.56
Caspase 3	*D86352*		3.21	4.92
Cytotoxic granule-associated RNA binding protein 1	*BG518542*		2.25	2.29
Nerve growth factor receptor P75	*BB151515*		1.97	2.15
Cell cycle				
Cyclin B1	*AU015121*	3.33	2.86	4.36
Myeloblastosis oncogene	*NM_033597*		1.91	1.91
N-Myc-related oncogene 1	*BC005453*		2.53	2.97
Matrix/structural				
Milk fat globule-EGF factor 8 protein	*NM_008594*	2.06	2.13	2.45
Chondroitin sulfate proteoglycan 3	*BM945195*		2.01	3.59
Thymosin, beta 10	*AV148480*		3.85	6.00
Protein synthesis				
CUG triplet repeat, RNA binding protein 2	*AF090696*		2.23	2.13
Proteolysis				
Calpain 7	*BG068214*		1.87	1.88
Matrix metalloproteinase 9	*AW541504*	2.09		
Signal transduction				
Cyclin-dependent kinase 5, regulatory subunit (p35)	*BB526485*		1.86	1.93
Cyclin-dependent kinase inhibitor 1A (P21)	*AK007630*		2.22	2.58
Fyn proto-oncogene	*BG074018*	1.90		
Growth associated protein 43	*BB622036*	7.03	7.60	12.74
Protein kinase inhibitor, alpha	*AK010212*		2.82	4.22
PKA, type II beta	*BG071003*	4.58		
Somatostatin	*NM_009215*		3.17	5.67
Transcription/chromatin				
Aryl-hydrocarbon receptor	*NM_013464*		1.90	2.47
BTB and CNC homology 2	*AW553304*		1.97	2.88
High mobility group box 2	*C85885*	3.87	3.29	4.15
Myelocytomatosis oncogene (c-myc)	*BC006728*	2.29	1.97	1.96
SRY-box containing gene 4	*AI428101*		3.26	6.41
TGFB inducible early growth response 1	*NM_013692*		1.85	2.55
Unknown				
Prion protein dublet	*BG086022*	2.24		

[1]Listed are genes with possible roles in cell death increased during the critical period in the CN at P7 compared to after the critical period at P14 and P21. Differential expression was defined by ≥1.8-fold change and an FDR adjusted *P*-value ≤0.05. Genes are arranged by broad functional categories. The GenBank accession numbers and the fold change ratios determined from the NIA and Affymetrix analyses are also shown. Many of the differentially expressed genes were identified on both types of arrays, some genes were identified from only the NIA or Affymetrix analyses.

SERCA2 (ATPase Ca++ transporting, cardiac muscle, slow twitch) calcium pump functions to maintain appropriate calcium levels across the endoplasmic reticulum membrane. Other calcium-binding proteins, calretinin and parvalbumin, were also increased in the CN after the critical period. Calcium homeostasis is known to play a role in tipping the balance of apoptotic or survival pathways and these increases in calcium regulatory genes may make mature neurons more capable of dealing with sudden changes in calcium concentration.

Finally, members of various signal transduction pathways with known roles in protection against apoptosis were higher after the critical period. This included receptors such as endothelial deafferentation sphingolipid G-protein coupled receptors 1 and 8, which inhibit ceramide-induced death, as well as the interleukin 10 alpha receptor, which can inhibit glutamate mediated neuron death (Bachis et al., 2001; Cuvillier, 2002). This also included the protective serum regulated kinase as well as a 14-3-3 protein family member, which could bind pro-apoptotic genes such as Bad to prevent apoptosis (Brunet et al., 2001; Berg et al., 2003).

Microarray validation and immunohistochemistry

To validate the mRNA expression changes measured using microarrays, 18 genes were chosen that met the criteria for differential expression from Tables 3 and 4, and four more genes were chosen that showed a fold change ratio of less than 1.8 on the microarrays, but still had an FDR corrected *P*-value ≤ 0.05. Real-time RT-PCR was performed using P7 and P21 CN as templates for comparison. Shown in Figure 6, the microarray analyses for P7 compared to P21 were consistent with the direction of change in the PCR results for 21 out of 22 genes. This included the four genes with a microarray fold change of less than 1.8, but with a significant *P*-value (Bcl-w, Bcl-x, Bok, and Caspase 7). The magnitude of the fold changes measured with PCR was also consistent with the array results, with the exception of metallothionein I. The neurotrophin receptor p75 appeared to be a false-positive on the array because PCR analysis suggested there was no reliable change between P7 and P21 CN in p75 mRNA expression, while the array results showed a fold

TABLE 4. Candidate Genes Expressed Higher after the Critical Period[1]

Gene name	*Accession number*	NIA ratio P21/P7	Affy ratio P14/P7	Affy ratio P21/P7
Energy/metabolism				
Glutathione synthetase	*BG067069*	2.01		
Peroxiredoxin 6	*BG064735*	2.19		
Selenoprotein X 1	*BG076434*	1.86		
Creatine kinase, mitochondrial 1, ubiquitous	*NM_009897*	2.32	2.09	2.14
Glutamine synthase	*U09114*		1.80	2.60
Glycine amidinotransferase	*AW108522*		2.11	2.97
Guanidinoacetate methyltransferase	*AF015887*		2.29	2.41
N-acylsphingosine amidohydrolase 2	*NM_018830*	2.79	2.11	2.12
Prion protein	*BE630020*		2.05	2.30
Heat shock/stress				
Heat shock protein 105	*BG064500*	2.01		
Oxidation resistance 1	*BG087025*	1.96		
Crystallin, alpha B	*NM_009964*	5.73	4.36	1.97
Heat-responsive protein 12	*AK005016*	2.79	2.65	2.05
Metallothionein 1	*NM_013602*	5.47	3.08	3.35
Metallothionein 2	*AA796766*	5.26	2.70	3.09
Ion transport				
ATPase, Ca++ transporting, cardiac muscle, slow twitch 2	*BG085195*	2.01		
ATPase, Na+/K+ transporting, alpha 2 polypeptide	*BQ175915*		3.05	3.23
Glutamate receptor, ionotropic, NMDA2C (epsilon 3)	*NM_010350*		2.03	2.52
Matrix/structural				
CD59a antigen	*AK005507*		2.24	3.68
Gelsolin	*AV025667*	4.33	6.11	1.91
Tissue inhibitor of metalloproteinase 4	*BI788452*	2.89	2.23	2.52
Signal transduction				
Activity regulated cytoskeletal protein	*NM_018790*	2.88	2.14	2.06
Calbindin 2 (calretinin)	*BC017646*		1.89	2.01
Calcitonin/calcitonin-related polypeptide, alpha	*AF330212*		3.99	1.82
Cyclic nucleotide phosphodiesterase 1	*NM_009923*		2.69	1.90
Down syndrome critical region gene 1-like1	*NM_030598*		2.90	3.29
Endothelial deafferentation sphingolipid G-protein-coupled receptor 1	*BB133079*		2.45	2.43
Endothelial deafferentation, lysophosphatidic acid G-protein-coupled-receptor, 2	*U70622*	3.06	2.55	2.13
Endothelial deafferentation sphingolipid G-protein-coupled receptor, 8	*NM_053190*		3.96	2.33
Fibroblast growth factor 1	*BM932451*		3.60	2.75
Interleukin 10 receptor, alpha	*BG074640*	1.85		
Parathyroid hormone-like peptide	*NM_008970*	2.78	3.65	3.65
Parvalbumin	*NM_013645*		2.52	2.53
Phosphatidylinositol 3-kinase, regulatory subunit, polypeptide 1 (p85 alpha)	*BG081616*	2.30		
Serum/glucocorticoid regulated kinase	*BG072439*	2.40		
14-3-3 (eta polypeptide)	*BG065012*	1.92		
Transcription/chromatin				
Basic helix-loop-helix domain containing, class B2	*NM_011498*		2.06	2.49
Delta sleep inducing peptide, immunoreactor	*AF201289*		1.86	3.79
Transport				
Solute carrier family 1 (glial high affinity glutamate transporter), member 2	*U75372*		1.96	2.58

[1]Listed are genes with possible roles in cell survival increased after the critical period in the CN at P14 and P21 compared to during the critical period at P7. Differential expression was defined by ≥1.8-fold change and an FDR adjusted *P*-value ≤ 0.05. Genes are arranged by broad functional categories. The GenBank accession numbers and the fold change ratios determined from the NIA and Affymetrix analyses are also shown. Many of the differentially expressed genes were identified on both types of arrays, some genes were identified from only the NIA or Affymetrix analyses.

change of 2.15 (note the lack of a black bar for P75 in Fig. 6).

Protein expression of a subset of differentially expressed genes was analyzed for three reasons. First, to determine if mRNA expression differences correlated with protein expression differences between P7 and P21 CN; second, to determine which or if all of the three subdivisions of the CN (anteroventral CN, posteroventral CN, and dorsal CN; AVCN, PVCN, and DCN) show the difference; and finally, to determine what cell types were expressing these genes. Protein expression for the six genes examined correlated well with the mRNA differences observed in the microarray data. Figure 7 shows representative images of immunohistochemical labeling for three proteins in AVCN that are more highly expressed during the critical period relative to later in development. Pro-caspase 3 expression was qualitatively higher throughout the entire P7 CN compared to P21, with the exception of an area in the posteroventral CN (data not shown). A representative example of pro-caspase 3 labeling in the AVCN is shown in Figure 7A,B. At P7 pro-caspase 3 was expressed in a variety of neuron types, including granule cells and spher-

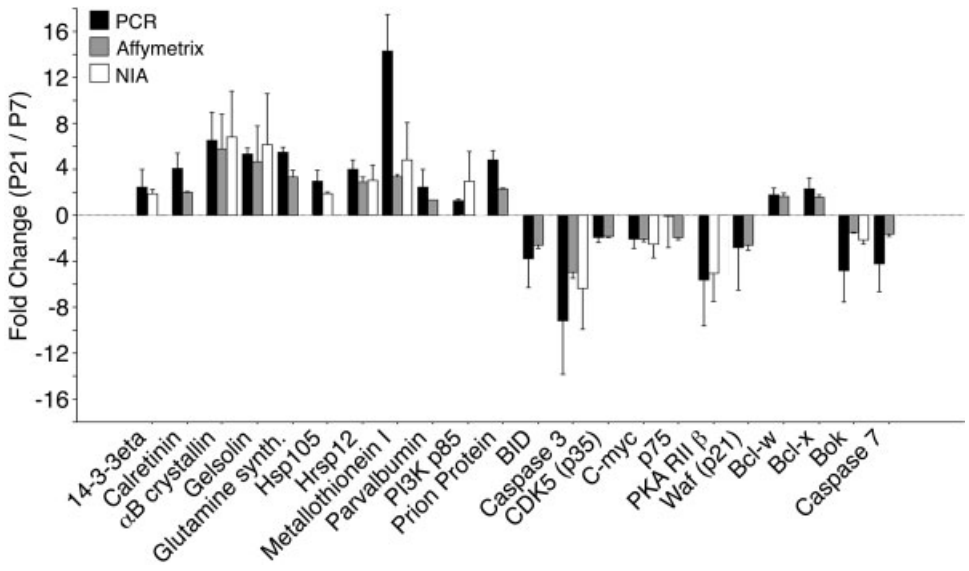

Fig. 6. Confirmation of microarray results for 22 genes using real-time RT-PCR. Each bar represents the fold change ratio of P7 compared to P21 measured using PCR (black), Affymetrix (gray), and/or NIA (white) microarray analyses. Genes identified as differentially expressed on only one of the two platforms have two bars (one array and PCR). PCR fold change ratios were computed with the relative C_T method using the ribosomal protein L3 for normalization. Microarray and PCR analyses generally showed consistent changes, the p75 neurotrophin receptor was one exception (note the black bar is approximately zero). Error bars indicate 1 SD.

ical bushy cells, based on cell size and location within the CN, it may also be in glia (Fig. 7A, inset). The inhibitory PKA subunit RIIβ protein also appeared to be expressed higher throughout the entire P7 CN compared to P21. A representative example of labeling in AVCN is shown in Figure 7C,D. PKARIIβ was also expressed in neurons based on size and location within the CN (inset, Fig. 7C). Finally, the transcription factor c-myc appeared to be expressed at a higher level in all areas of the CN at P7 relative to P21. A representative example of c-myc labeling in AVCN is shown in Figure 7E,F. C-myc appeared to be predominantly expressed in neurons at both ages, but was also observed in glial cells (inset, Fig. 7E). The expression of phosphorylated c-myc in the P7 and P21 CN was also analyzed with immunohistochemistry and showed a similar staining pattern (see Supplemental Material).

Figure 8 shows representative images of immunohistochemistry labeling for three proteins in AVCN that are more highly expressed after the critical period relative to earlier in development. The small heat shock protein, αB crystallin, was expressed throughout the CN at P21 compared to P7, where no labeling was observed, shown in Figure 8A,B. The cells that expressed αB crystallin appeared to be small neurons, based on morphology. It was not expressed in any of the larger neurons, such as bushy cells (Fig. 8B, inset). Figure 8C,D shows labeling with an antibody that detects metallothionein isoforms I and II (MT I/II). MT I/II shows more labeling throughout the P21 CN compared to P7, where almost no labeling was observed. The MT I/II-positive cells did not appear to be neurons. These small, rounded cells were found in close association with the larger neurons and may be satellite glial cells (Fig. 8D, inset). Finally, parvalbumin was highly expressed in neurons of both P7 and P21 AVCN and PVCN (data not shown). However, parvalbumin expression was much higher in the DCN at P21 compared to P7, as shown in Figure 8E,F, so that overall the mRNA fold change measured using microarrays is paralleled by overall protein expression. Parvalbumin protein expression in DCN appeared in almost every cell type (Fig. 8F, inset).

Analysis of known apoptotic genes represented on either array platform

There have been relatively few reports of genes with known roles in apoptosis that are developmentally regulated in the brain during postnatal development (de Bilbao et al., 1999; Mooney and Miller, 2000; Krajewska et al., 2002). Therefore, to explore this trend in relation to the critical period studied here, genes represented on the array platforms with established roles in apoptosis, either pro-death or pro-survival, were selected and are shown in Table 5. Out of 22 pro-apoptotic genes surveyed, seven were differentially expressed over these postnatal ages. Strikingly, six out of these seven pro-death genes were expressed more highly during the critical period at P7 when cells are susceptible to loss of afferent input, relative to later postnatal ages P14 and P21. Out of 23 anti-apoptotic genes surveyed, 11 were differentially expressed. Nine out of these 11 pro-survival genes were increased after the critical period at P14 and P21, when cells are resistant to loss of afferent input compared to expression at P7. The trend of increasing pro-survival and decreasing pro-death mechanisms is highly significant ($P < 0.005$ by chi-square) and correlates with the timing of age-dependent susceptibility to loss of afferent input.

DISCUSSION

The mechanisms that regulate the timing of critical periods during nervous system development are not well

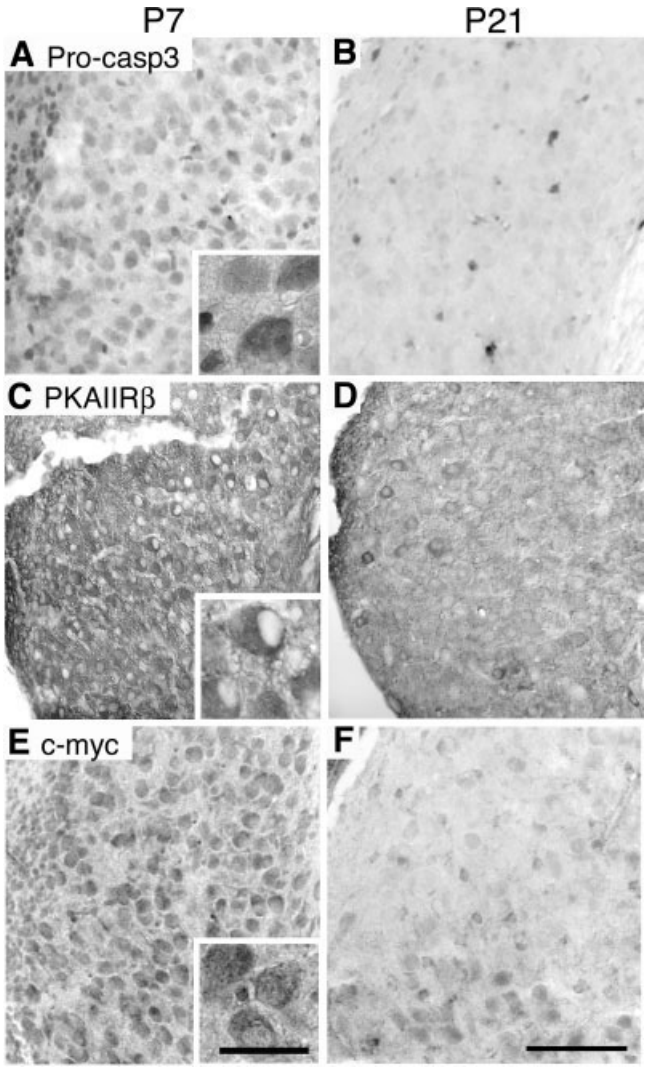

Fig. 7. Immunohistochemistry of protein from three genes that array data indicated as more highly expressed in the CN during the critical period (P7) compared to after the critical period (P14 and P21). **A,B:** Representative sections of AVCN labeled for pro-caspase 3 at P7 and P21. More cells appear pro-caspase 3-positive at P7 compared to P21. Many of the labeled cells are neurons, based on size and position (inset, A). **C,D:** Representative sections of AVCN labeled for the PKA type II regulatory subunit β at P7 and P21. PKARIIβ labeling is much higher at P7 compared to P21 and also appears to be expressed in neurons (inset, C). **E,F:** Representative sections of AVCN labeled for c-myc at P7 and P21. C-myc is expressed at a higher level at P7 compared to P21, and the labeled cells appear to be mostly neurons and some glial cells (inset, E). Scale bars = 100 μm in F (applies to A–F); 25 μm in inset E (applies to inset A,C,E).

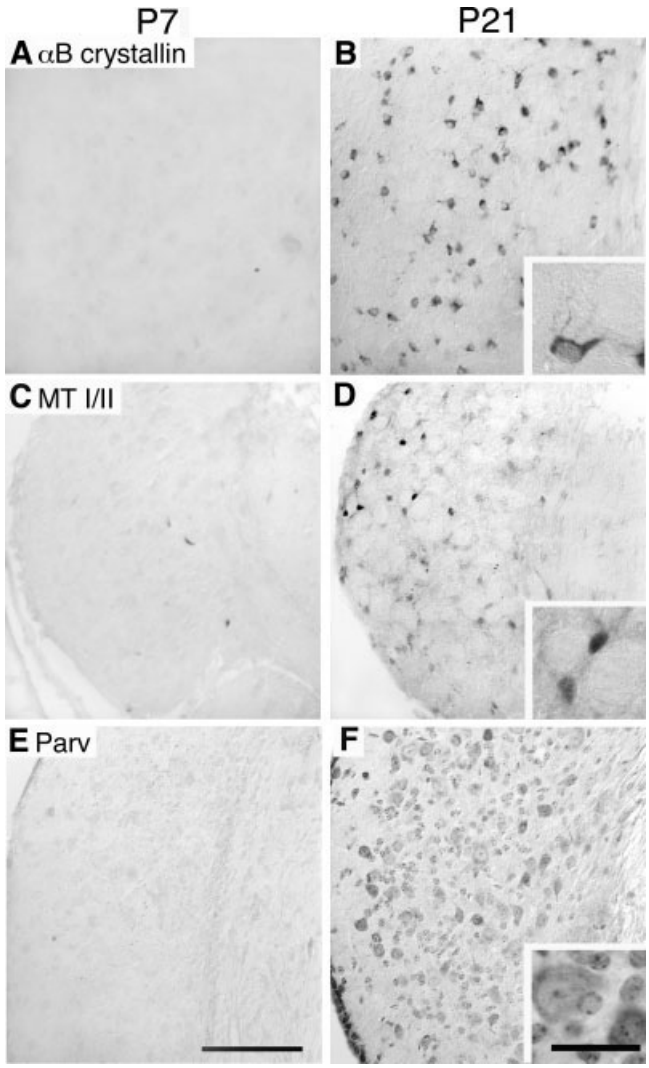

Fig. 8. Immunohistochemistry of protein from three genes that array data indicated as more highly expressed in the CN after the critical period (P14 and P21) compared to during the critical period (P7). **A,B:** Representative sections of AVCN labeled for αB crystallin at P7 and P21. Notice the absence of any labeling at P7 and many cells immunopositive at P21. The labeled cells are likely neurons based on morphology, but are not the larger bushy neurons typical of this region (inset, B). **C,D:** Representative sections of AVCN labeled for metallothionein I/II at P7 and P21. MT I/II labeling is much higher at P21 compared to P7, where there is a noticeable lack of any immunopositive cells. MT I/II does not appear to be expressed in neurons, but in glial cells found in apposition to neurons (inset D). **E,F:** Representative sections of DCN labeled for parvalbumin at P7 and P21. Parvalbumin is expressed much higher at P21 compared to P7 in DCN, but not in VCN (not shown), and appears to be expressed in many different cell types (inset F). Scale bars = 100 μm in A (applies to A–F); 25 μm in inset F (applies inset B,D,F).

understood, although this information may be more accessible with advances in experimental technologies (Hensch, 2004). Here we used microarray technology to survey for differences in baseline gene expression over three postnatal ages that define a critical period of afferent-dependent neuron survival in the mouse cochlear nucleus. Using two different microarray platforms, we identified more than 1,000 genes (including named genes and ESTs) with a variety of functions that change in relative expression level from 1–3 weeks postnatal in parallel with the timing of this critical period. For a subset of genes we verified the microarray estimates of mRNA fold change using real-time RT-PCR, and we further explored the protein expression and localization of several identified candidate genes. Finally, we described a striking correlation between postnatal age, susceptibility to afferent deprivation, and relative expression of cell death and survival genes.

TABLE 5. Summary of Apoptotic Genes on Both the NIA and Affymetrix Arrays

	Critical period	Postcritical period		Critical period	Postcritical period
Pro-apoptotic			**Anti-apoptotic**		
AIF			AlphaB Crystallin		√√
AIP-1 (alix)		√√	A1		
Apaf-1			API5		
Bad			Bcl-2		
Bak1			Bcl-w		√
Bax			Bcl-x		√
Bid	√√		Boo/Diva		
Bik			CREB		
Bim			Gelsolin		√√
Bok	√		Hsp12		√√
CAD			Hsp25	√	
Caspase 12			Hsp70		
Caspase 3	√√		Hsp105		√√
Caspase 6			IAP1		
Caspase 7	√		ICAD		
Caspase 8			Mcl-1		
Caspase 9			Mef2d		√
Cytochrome c			Metallothionein I		√√
DP5, Hrk			Metallothionein II		√√
P53	√		Naip		
P75	√√		NF κ B		
Smac/Diablo			Survivin	√√	
			Xiap		

Genes with established pro- and anti-apoptotic roles that are represented on either the NIA mouse 15K cDNA or Affymetrix Mouse 430A microarray are listed. In a survey of these genes, 6 out of 7 with pro-apoptotic roles were expressed higher during the critical period at P7, 9 out of 11 differentially expressed genes with anti-apoptotic roles were expressed higher after the critical period at P14 and P21. Differentially expressed genes are indicated with either a √ or √√. The √√ indicates fold change ≥1.8 and FDR adjusted *P*-value ≤ 0.05. The √ indicates fold change < 1.8, but still with FDR adjusted *P*-value ≤ 0.05. Unmarked genes did not show any reliable differences in expression between P7 and P14 or P21.

Comparison across microarray platforms

A widespread diversity of array technologies are used by different researchers and laboratories, making comparisons across platforms of general interest to the scientific community. By using two different microarray technologies to compare gene expression between ages in the mouse CN, we were able to analyze the amount of correlation in our results across platforms. In agreement with previous work comparing Affymetrix with cDNA microarrays, we found a fairly low correlation between fold changes over all the shared genes. This correlation increased substantially when low-intensity genes were removed from the analysis (Park et al., 2004; Shippy et al., 2004). However, regardless of signal intensity used to derive the fold change ratios, the correlation across platforms in our study also improved substantially for genes showing larger fold changes. This has not been reported previously to the best of our knowledge and is encouraging for investigators who wish to compare results of their own identified differentially expressed genes across platforms.

Development of the cochlear nucleus

In addition to identifying candidate genes related to the critical period under investigation, gene array analysis provided insights into normal development of the CN. We identified both new patterns of gene expression and broad changes in functions that might be expected based on previous studies. The representation of different functional categories during and after the critical period appeared to reflect the maturation state of the CN. For example, one of the largest differences in function represented by genes increased at P7 was cell-cycle-related genes. This change might reflect gene expression in glial cells, as it is known that glial cells in the CN continue to proliferate and differentiate well into the first postnatal week (Martin and Rickets, 1981). The expression of specific cell-cycle genes in different cell types still needs to be analyzed. Energy, metabolism, ion transport, and signal transduction genes were more prevalent at P14 and P21, after the onset of hearing (P10–12; Ehret, 1976). An increase in mRNAs involved in these functions might be expected as indicative of mature functioning neurons with higher metabolic demands and the machinery to transmit electrical signals. While these differences in functions may not be unexpected, these results of the microarray comparisons have not been demonstrated previously in the developing auditory brainstem.

We identified genes not previously known to be expressed in the CN and described their regulation over postnatal development. Several genes identified in the CN in our study are also regulated in other brain areas over the same postnatal ages. Out of the 66 genes listed in Tables 3 and 4, 29 change in either protein or mRNA expression level over the first 3 postnatal weeks in other areas of the CNS, including: caspase 3, cdk5(p35), p75, fibroblast growth factor 1, metallothionein I and II, and creatine kinase (Thomas et al., 1991; Chen et al., 1994; Tomizawa et al., 1996; Yakovlev et al., 2001; Boero et al., 2003; Natale et al., 2004). In addition to our validations using real-time RT-PCR and immunohistochemistry, our microarray results are validated by comparisons to previous findings. For example, parvalbumin and gap43 have been specifically shown to be regulated in the rodent CN over the same ages we demonstrated here (Lohmann and Friauf, 1996; Illing et al., 1999).

Analysis of potential critical period regulation genes

A surprising and conceptually interesting finding is that the numbers of genes up- or downregulated were very similar for P7 compared with both P14 and P21. In contrast, there were remarkably few genes either up- or downregulated between P14 and P21, both ages after the end of this critical period and the onset of hearing, but

during marked changes in hearing efficacy. The possibility of a link between genes underlying functional maturation and survival independent of afferent input is supported by this pattern of expression. This database of over 1,000 genes regulated around the onset of hearing and the end of the critical period in the CN provides a rich resource for the generation of many new hypotheses about the molecular mechanisms underlying this and other critical periods of neural maturation. Both the Affymetrix and cDNA datasets have been deposited in a public database in their entirety (www.ncbi.nlm.nih.gov/geo/, series number GSE2390).

We focused on selecting candidate genes that are most likely involved in cell death or survival based on published literature. This may seem restrictive, but it still provided a list of genes with well-established roles in cell death, such as caspase 3, and others with less well-established roles, such as the PKA type II regulatory subunit β, that we would not have anticipated to be regulated in the CN (Elliott et al., 2003). This restriction led to an initial set of 66 candidates for further analysis. The question remains if any of these genes are the molecules both necessary and sufficient for the critical period response to deafferentation or if they play some other unrelated developmental role. Validation by real-time RT-PCR and protein localization is an important step in further refining the candidate list. With a few exceptions, the validations we have done to date supported the differential expression of mRNA and protein level.

One outcome of this study is the identification of single genes whose changes in expression correlate with the timing of this critical period in the mouse CN. There are compelling arguments for the potential involvement of any of the genes listed in Tables 3 and 4 in defining the critical period response. For example, the higher baseline expression of caspase 3 mRNA and protein in the P7 CN compared to P14 and P21 CN could certainly predispose those neurons to a faster and easier death following the loss of afferent input or another metabolic challenge. Specifically, a viable hypothesis is that cells with a smaller pool of caspase 3 ready to be activated have more time to mount a survival response and will be protected against an apoptotic insult. In this example, we propose the possibility that a single gene could underlie this age-dependent susceptibility to loss of afferent input. On the other hand, the results shown in Table 5 lead us to speculate that it is more likely a cohort of genes regulated over development that mediate this switch from afferent-dependent to -independent neuronal survival. The specific genes that make up this cohort remain to be studied further by manipulating gene expression or function and analyzing the effects on the critical period response to cochlear removal.

A striking result of these studies was the higher expression of known pro-apoptotic genes during the critical period at P7 and, conversely, the higher expression of pro-survival genes after the critical period at P14 and P21. This result suggests a developmental trend of increasing protective mechanisms and decreasing pro-death mechanisms that corresponds to this period of age-dependent susceptibility. We hypothesize that this could be a general phenomenon of nervous system development, and other recent reports support this possibility (Benn and Woolf, 2004; Walsh et al., 2004). In addition, it is reminiscent of other mechanisms of neuronal homeostasis that could function to maintain the integrity and organization of local circuits in the CNS (Mizrahi and Katz, 2003; Wierenga et al., 2005). Survival of many types of immature neurons is dependent on some form of trophic support, and death seems to be the default program if such support is not abundant. While mature neurons are obviously capable of dying, they are often less sensitive than immature neurons to the same insult. A developmental decline in pro-death genes and increase in pro-survival genes could underlie this common phenomenon and act as a homeostatic mechanism to keep mature neurons alive, promoting stability in the connections of the brain for the lifetime of the organism.

ACKNOWLEDGMENTS

We thank Dr. Mark Whipple for helpful discussions on microarray data analysis and Rachel Nehmer for excellent technical assistance.

LITERATURE CITED

Ashburner M, Ball CA, Blake JA, Botstein D, Butler H, Cherry JM, Davis AP, Dolinski K, Dwight SS, Eppig JT, Harris MA, Hill DP, Issel-Tarver L, Kasarskis A, Lewis S, Matese JC, Richardson JE, Ringwald M, Rubin GM, Sherlock G. 2000. Gene ontology: tool for the unification of biology. The Gene Ontology Consortium. Nat Genet 25:25–29.

Bachis A, Colangelo AM, Vicini S, Doe PP, De Bernardi MA, Brooker G, Mocchetti I. 2001. Interleukin-10 prevents glutamate-mediated cerebellar granule cell death by blocking caspase-3-like activity. J Neurosci 21:3104–3112.

Baldi A, Calia E, Ciampini A, Riccio M, Vetuschi A, Persico AM, Keller F. 2000. Differentiation-induced apoptosis of neurons in thalamic somatosensory nuclei of the newborn rat: critical period and rescue from cell death by peripherally applied neurotrophins. Eur J Neurosci 12:2281–2290.

Bamji SX, Majdan M, Pozniak CD, Belliveau DJ, Aloyz R, Kohn J, Causing CG, Miller FD. 1998. The p75 neurotrophin receptor mediates neuronal apoptosis and is essential for naturally occurring sympathetic neuron death. J Cell Biol 140:911–923.

Benn SC, Woolf CJ. 2004. Adult neuron survival strategies—slamming on the brakes. Nat Rev Neurosci 5:686–700.

Berg D, Holzmann C, Riess O. 2003. 14-3-3 proteins in the nervous system. Nat Rev Neurosci 4:752–762.

Boero J, Qin W, Cheng J, Woolsey TA, Strauss AW, Khuchua Z. 2003. Restricted neuronal expression of ubiquitous mitochondrial creatine kinase: changing patterns in development and with increased activity. Mol Cell Biochem 244:69–76.

Born DE, Rubel EW. 1985. Afferent influences on brain stem auditory nuclei of the chicken: neuron number and size following cochlea removal. J Comp Neurol 231:435–445.

Brunet A, Park J, Tran H, Hu LS, Hemmings BA, Greenberg ME. 2001. Protein kinase SGK mediates survival signals by phosphorylating the forkhead transcription factor FKHRL1 (FOXO3a). Mol Cell Biol 21: 952–965.

Brustovetsky N, Brustovetsky T, Dubinsky JM. 2001. On the mechanisms of neuroprotection by creatine and phosphocreatine. J Neurochem 76: 425–434.

Chen CK, Kinsman SL, Holtzman DM, Mobley WC, Johnston MV. 1994. A reverse transcription-polymerase chain reaction study of p75 nerve growth factor receptor gene expression in developing rat cerebellum. Int J Dev Neurosci 12:255–262.

Cuvillier O. 2002. Sphingosine in apoptosis signaling. Biochim Biophys Acta 1585:153–162.

de Bilbao F, Guarin E, Nef P, Vallet P, Giannakopoulos P, Dubois-Dauphin M. 1999. Postnatal distribution of cpp32/caspase 3 mRNA in the mouse central nervous system: an in situ hybridization study. J Comp Neurol 409:339–357.

Ehret G. 1976. Development of absolute auditory thresholds in the house mouse (Mus musculus). J Am Audiol Soc 1:179–184.

Elliott MR, Tolnay M, Tsokos GC, Kammer GM. 2003. Protein kinase A

regulatory subunit type II beta directly interacts with and suppresses CREB transcriptional activity in activated T cells. J Immunol 171: 3636–3644.

Gafni J, Hermel E, Young JE, Wellington CL, Hayden MR, Ellerby LM. 2004. Inhibition of calpain cleavage of huntingtin reduces toxicity: accumulation of calpain/caspase fragments in the nucleus. J Biol Chem 279:20211–20220.

Galli-Resta L, Ensini M, Fusco E, Gravina A, Margheritti B. 1993. Afferent spontaneous electrical activity promotes the survival of target cells in the developing retinotectal system of the rat. J Neurosci 13:243–250.

Giralt M, Penkowa M, Lago N, Molinero A, Hidalgo J. 2002. Metallothionein-1+2 protect the CNS after a focal brain injury. Exp Neurol 173:114–128.

Hanayama R, Tanaka M, Miwa K, Shinohara A, Iwamatsu A, Nagata S. 2002. Identification of a factor that links apoptotic cells to phagocytes. Nature 417:182–187.

Hashisaki GT, Rubel EW. 1989. Effects of unilateral cochlea removal on anteroventral cochlear nucleus neurons in developing gerbils. J Comp Neurol 283:5–73.

Hatayama T, Yamagishi N, Minobe E, Sakai K. 2001. Role of hsp105 in protection against stress-induced apoptosis in neuronal PC12 cells. Biochem Biophys Res Commun 288:528–534.

Hensch TK. 2004. Critical period regulation. Annu Rev Neurosci 27:549–579.

Illing RB, Cao QL, Forster CR, Laszig R. 1999. Auditory brainstem: development and plasticity of GAP-43 mRNA expression in the rat. J Comp Neurol 412:353–372.

Irizarry RA, Hobbs B, Collin F, Beazer-Barclay YD, Antonellis KJ, Scherf U, Speed TP. 2003. Exploration, normalization, and summaries of high density oligonucleotide array probe level data. Biostatistics 4:249–264.

Jourquin J, Tremblay E, Decanis N, Charton G, Hanessian S, Chollet AM, Le Diguardher T, Khrestchatisky M, Rivera S. 2003. Neuronal activity-dependent increase of net matrix metalloproteinase activity is associated with MMP-9 neurotoxicity after kainate. Eur J Neurosci 18:1507–1517.

Kalb R. 2005. The protean actions of neurotrophins and their receptors on the life and death of neurons. Trends Neurosci 28:5–11.

Kamradt MC, Chen F, Cryns VL. 2001. The small heat shock protein alpha B-crystallin negatively regulates cytochrome c- and caspase-8-dependent activation of caspase-3 by inhibiting its autoproteolytic maturation. J Biol Chem 276:16059–16063.

Kamradt MC, Chen F, Sam S, Cryns VL. 2002. The small heat shock protein alpha B-crystallin negatively regulates apoptosis during myogenic deafferentation by inhibiting caspase-3 activation. J Biol Chem 277:38731–38736.

Kargul GJ, Dudekula DB, Qian Y, Lim MK, Jaradat SA, Tanaka TS, Carter MG, Ko MS. 2001. Verification and initial annotation of the NIA mouse 15K cDNA clone set. Nat Genet 28:17–18.

Krajewska M, Mai JK, Zapata JM, Ashwell KW, Schendel SL, Reed JC, Krajewski S. 2002. Dynamics of expression of apoptosis-regulatory proteins Bid, Bcl-2, Bcl-X, Bax and Bak during development of murine nervous system. Cell Death Differ 9:145–157.

Kuo WP, Jenssen TK, Butte AJ, Ohno-Machado L, Kohane IS. 2002. Analysis of matched mRNA measurements from two different microarray technologies. Bioinformatics 18:405–412.

Levi-Montalcini R. 1949. Development of the acousticovestibular centers in the chick embryo in the absence of the afferent root fibers and of descending fiber tracks. J Comp Neurol 91:209–242.

Liu DX, Biswas SC, Greene LA. 2004. B-myb and C-myb play required roles in neuronal apoptosis evoked by nerve growth factor deprivation and DNA damage. J Neurosci 24:8720–8725.

Lohmann C, Friauf E. 1996. Distribution of the calcium-binding proteins parvalbumin and calretinin in the auditory brainstem of adult and developing rats. J Comp Neurol 367:90–109.

Martin MR, Rickets C. 1981. Histogenesis of the cochlear nucleus of the mouse. J Comp Neurol 197:169–184.

Matikainen T, Perez GI, Jurisicova A, Pru JK, Schlezinger JJ, Ryu HY, Laine J, Sakai T, Korsmeyer SJ, Casper RF, Sherr DH, Tilly JL. 2001. Aromatic hydrocarbon receptor-driven Bax gene expression is required for premature ovarian failure caused by biohazardous environmental chemicals. Nat Genet 28:355–360.

Mizrahi A, Katz LC. 2003. Dendritic stability in the adult olfactory bulb. Nat Neurosci 6:1201–1207.

Mooney SM, Miller MW. 2000. Expression of bcl-2, bax, and caspase-3 in the brain of the developing rat. Brain Res Dev Brain Res 123:103–117.

Moore DR. 1990. Auditory brainstem of the ferret: early cessation of developmental sensitivity of neurons in the cochlear nucleus to removal of the cochlea. J Comp Neurol 302:810–823.

Mostafapour SP, Cochran SL, Del Puerto NM, Rubel EW. 2000. Patterns of cell death in mouse anteroventral cochlear nucleus neurons after unilateral cochlea removal. J Comp Neurol 426:561–571.

Mostafapour SP, Del Puerto NM, Rubel EW. 2002. bcl-2 overexpression eliminates deprivation-induced cell death of brainstem auditory neurons. J Neurosci 22:4670–4674.

Natale JE, Knight JB, Cheng Y, Rome JE, Gallo V. 2004. Metallothionein I and II mitigate age-dependent secondary brain injury. J Neurosci Res 78:303–314.

Park KT, Mitchell KA, Huang G, Elferink CJ. 2005. The Ah receptor predisposes hepatocytes to fas-mediated apoptosis. Mol Pharmacol 612–622.

Park PJ, Cao YA, Lee SY, Kim JW, Chang MS, Hart R, Choi S. 2004. Current issues for DNA microarrays: platform comparison, double linear amplification, and universal RNA reference. J Biotechnol 112: 225–245.

Reiner A, Yekutieli D, Benjamini Y. 2003. Identifying differentially expressed genes using false discovery rate controlling procedures. Bioinformatics 19:368–375.

Sanes DH, Walsh EJ. 1998. The development of central auditory processing. In: Rubel EW, Popper AN, Fay RR, editors. Development of the auditory system. New York: Springer. p 271–314.

Shippy R, Sendera TJ, Lockner R, Palaniappan C, Kaysser-Kranich T, Watts G, Alsobrook J. 2004. Performance evaluation of commercial short-oligonucleotide microarrays and the impact of noise in making cross-platform correlations. BMC Genomics 5:61.

Tanaka TS, Jaradat SA, Lim MK, Kargul GJ, Wang X, Grahovac MJ, Pantano S, Sano Y, Piao Y, Nagaraja R, Doi H, Wood WH, 3rd, Becker KG, Ko MS. 2000. Genome-wide expression profiling of mid-gestation placenta and embryo using a 15,000 mouse developmental cDNA microarray. Proc Natl Acad Sci U S A 97:9127–9132.

Thomas D, Groux-Muscatelli B, Raes MB, Caruelle JP, Stehelin D, Barritault D, Boilly B. 1991. Developmental changes of acidic fibroblast growth factor (aFGF) transcription and expression in mouse brain. Brain Res Dev Brain Res 59:117–122.

Tierney TS, Russell FA, Moore DR. 1997. Susceptibility of developing cochlear nucleus neurons to deafferentation-induced death abruptly ends just before the onset of hearing. J Comp Neurol 378:295–306.

Tomizawa K, Matsui H, Matsushita M, Lew J, Tokuda M, Itano T, Konishi R, Wang JH, Hatase O. 1996. Localization and developmental changes in the neuron-specific cyclin-dependent kinase 5 activator (p35nck5a) in the rat brain. Neuroscience 74:519–529.

Trune DR. 1982. Influence of neonatal cochlear removal on the development of mouse cochlear nucleus. I. Number, size, and density of its neurons. J Comp Neurol 209:409–424.

Walsh GS, Orike N, Kaplan DR, Miller FD. 2004. The invulnerability of adult neurons: a critical role for p73. J Neurosci 24:9638–9647.

Weishaupt JH, Kussmaul L, Grotsch P, Heckel A, Rohde G, Romig H, Bahr M, Gillardon F. 2003. Inhibition of CDK5 is protective in necrotic and apoptotic paradigms of neuronal cell death and prevents mitochondrial dysfunction. Mol Cell Neurosci 24:489–502.

Wierenga CJ, Ibata K, Turrigiano GG. 2005. Postsynaptic expression of homeostatic plasticity at neocortical synapses. J Neurosci 25:2895–2905.

Yakovlev AG, Ota K, Wang G, Movsesyan V, Bao WL, Yoshihara K, Faden AI. 2001. Differential expression of apoptotic protease-activating factor-1 and caspase-3 genes and susceptibility to apoptosis during brain development and after traumatic brain injury. J Neurosci 21: 7439–7446.

Zhu S, Li M, Figueroa BE, Liu A, Stavrovskaya IG, Pasinelli P, Beal MF, Brown RH Jr, Kristal BS, Ferrante RJ, Friedlander RM. 2004. Prophylactic creatine administration mediates neuroprotection in cerebral ischemia in mice. J Neurosci 24:5909–5912.